Int. J. Electrochem. Sci., 8 **(2013)** 8126 - 8137

International Journal of
ELECTROCHEMICAL
SCIENCE
www.electrochemsci.org

Investigation of the Corrosion Resistance of some Safely Additives and Mixed Salts – Scales on S41000 Stainless Steel Surface in Synthetic Seawater

Khadijah M. Emran[1,*], *Samia K. Hamdona*[2], *Abeer Mohammed Al Balawi*[1]

[1]Applied Chemistry Department, College of Applied Science, Taibaj University, Al-Madinah Al-Monawarah, Kingdom of Saudi Arabia.
[2] National Institute of Oceanography and Fisheries, Alexandria Egypt.
[*]E-mail: kabdalsamad@taibahu.edu.sa

Received: 4 April 2013 / *Accepted:* 14 May 2013 / *Published:* 1 June 2013

Formation of mineral scales of $CaCO_3$ and $CaSO_4$ poses significant problems in cooling water systems. During the precipitation of mixed $CaCO_3$ and $CaSO_4$ salts, Tyrosine (Tyr), polyacrylic acid (PAA) and yeast were used as anticorrosion of S41000 stainless steel in artificial seawater. In absence of additive, the oxygen reduction occurs in the pores formed between the scale crystals and metallic surface. The anticorrosion properties of these compound in presence of mixed scales were studied through electrochemical methods. The results show that yeast acts as a very good anticorrosion inhibitor. The beneficial effect of yeast compare with PAA and Tyr is due to its composition.

Keywords: A. stainless steel; B. EIS; B. polarization; C. high temperature corrosion; C. oxygen reduction.

1. INTRODUCTION

The rapid increase of the world's population and the non-uniform distribution of fresh water around the world has motivated research into the development of desalination methods. Desalination of sea water offers great potential for increasing the availability of fresh water [1]. Two of the main problems of cooling systems are corrosion and scale phenomena. These phenomena have a great economic impact, since the first involves deterioration of metallic surfaces by the medium, and the second causes loss of capacity for thermal exchange. Significant scientific and technological efforts have been made to control these phenomena, yet they are still controlled through addition of chemicals that inhibit their development [2-6]. Phosphorous free and less toxic scale inhibitors such as

polyacrylates and derivatives , various maleic , sulfonic acid , homo- and co-polymers are gaining importance. Some new chemistry was also proposed including natural and biodegradable compounds such as Carboxy Methyl Inulin and PolyAspartate and others [7-12].

Stainless steel (SS) grades commonly used to different types of desalination processes including seawater reverse osmosis and distillation. The behavior of stainless steels (SS) in aggressive environments is a major concern for designers and users. In seawater, SS corrosion is generally localized: pitting or crevice corrosion are generally reported. Extensive localized attack can lead to severe damage of the components [5].

The purpose of this paper is to study the corrosion resistance of some safely additives and mixed salts – scales on S41000 Stainless steel surface in synthetic seawater. The less toxic scale inhibitors such as additives: Tyrosine (Tyr), polyacrylic acid (PAA) and environmentally safe compound as yeast were used as anticorrosion . To our knowledge this is the first time that yeast has been used as inhibitor for corrosion process.

2. EXPERIMENTAL

The analytical reagents $CaCl_2$, Na_2SO_4, and Na_2CO_3 were dissolved in double distilled water and filtrates through membrane filters (0.22 μm Millipore) to produce super saturation of mixed salts - scales ($CaSO_4.2H_2O$ and $CaCO_3$ scales). For the mixed calcium sulphate and calcium carbonate system, the relative significance of the salts was determined with constant total calcium content (0.09M). Artificial seawater was prepared from reagent grade chemicals as record in the Table 1. The degree of salinity of this artificial seawater is 35 ‰[13].

Table 1. Major ions in seawater of salinity 35 ‰.

composition	NaCl	Na_2SO_4	KCl	$CaCl_2$	$MgCl_2$
$Mol.L^{-1}$	0.4266	0.0293	0.0106	0.0108	0.0552
g/Kg solution	24.061	4.011	0.761	1.153	5.069

Table 2. The composition of S41000 stainless steel (w%).

	Fe	Cr	P	S	Si	C	Mn
W%	Balance	13.5	0.40	0.035	1.0	0.15	1

Electrochemical measurements were performed at 25°C in a three-electrode cell containing 250 mL of electrolyte prepared immediately prior to each experiment. The working electrode was UNS S41000 stainless steels (S41000 SS) (1cm ×2.3cm) with chemical composition given in Table 2. The specimen was cleaned with emery paper and rinsed with bi-distilled water and ethanol (A.R) before

use. Pt counter electrode was oriented parallel to the working electrode. The potential was measured with respect to Saturated Calomel Electrode (SCE) reference electrode with a Luggin capillary positioned close and facing the study side of working electrode surface in order to minimize ohmic potential drop. ACM Gill AC instrument were used to acquire polarization and impedance data.

After immersion of the specimen in test solution(, prior to the impedance measurement, a stabilization period of 20 min was found, which proved sufficient for E_{ss} (the steady- state potential). The AC frequency rang extended from 30 kHz to 0.1 Hz, a 10 mV peak to peak sine, wave being the excitation signal. Potentiodynamic polarization curves were obtained with a potential sweep rate of 1 mV/s. The potential was sweep from cathodic to anodic directions after impedance run. The anticorrosion experiment carried out using 5 ppm of yeast, PAA and Try .

3.RESULTS AND DISCUSSION

3.1 Electrochemical behavior of S41000 SS in artificial sea water and mixed salts - scales .

Table 3. Numerical values of the impedance and polarization measurements for S41000 stainless steel in seawater at 25°C in absence and presence scale and additives.

Media	Impedance				Polarization			
	R_{ct} (Ωcm^2)	CPE ($\mu F/cm^2$)	n	IE.R_{ct}%	I_{corr} mA/cm^2	E_{pass} mV/SCE	I_{pass} mA/cm^2	IE.I_{corr} %
Seawater	25.06	13.78	0.76	-	1.070	-638 -146	0.033	-
Seawater + scale	33.72	8.41	0.80	25.68	0.829	-518	0.025	22.52
Yeast	45.82	6.15	0.76	35.88	0.659	-325	0.002	38.41
PAA	41.79	6.34	0.83	23.93	0.765	-297	0.00319	28.50
Tyr	37.66	6.19	0.72	11.68	0.936	-363	0.00267	12.52

Electrochemical results of S41000 SS in absence and presence of scale are shown in Fig.1. The Nuquit diagram (Fig.1,a) gave depressed capacitive loop in high frequency in absence and presence the scale with the theoretical center located below the real axis. This reflecting a surface inhomogeneity of structural or interfacial origin, such as those found in the adsorption processes. capacitive loop transfer to negative resistance at very low frequency in presence of scales. The capacitive loop in solution free of scale mainly due to the combination of the charge transfer resistance and the capacitance at the S41000 SS / solution interface (dielectric properties of the surface) [14] . These semicircles make an single angle (Θ_{max}) approaching 70º with the real axis in

bode plot (Fig.1,b). The tail at low frequency related to the diffusion process. The capacitive loop diameters and relaxation times become wider in presence of scale.

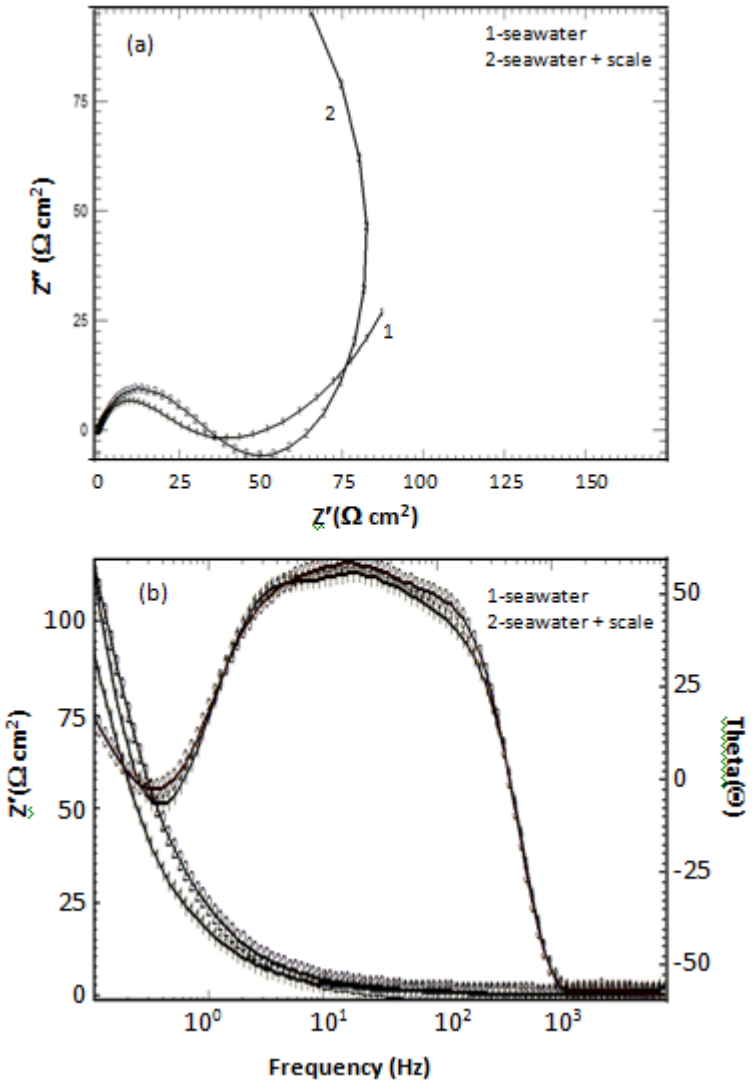

Figure 1. Impedance diagrams in Nyquist and bode plane plotted for S41000 SS in seawater without and with scale.

This means that the resistivity of the S41000 SS against the dissolution process become better as shown by R_{ct} values in Table 3. The first capacitive loop related with the dielectric properties of the formed film on the S41000 SS surface at the open circuit potential but it may also related to the electric double layer capacitance at the electrode / solution interface, which includes a S41000 SS / scale interface followed by a scale / solution interface. This increase in resistivity of S41000 SS is clearly associated by observation of a negative resistance at the low – frequency (negative impedance).

The transition of metal / solution interface from a state of active dissolution to the passive state is phenomenon of a great scientific and technological interest. This transition has been attributed to the formation of either a monolayer (or less) of absorbed oxygen on the surface, or to the coverage of

surface by a three – dimensional corrosion product or scales film. In either case, the reactive metal is shielded from the aqueous environment and the current drops sharply to a low value that is determined by the movement of ions or vacancies across the film. In the complex plane impedance diagram, the high frequency arm of the impedance is typical of a resistive / capacitive system, but the impedance locus terminates in a negative differential resistance as $\omega \rightarrow 0$. At higher potentials, the high – frequency locus is again dominated by an apparent resistive / capacitive response, but the low – frequency arm is not observed to terminate at the real axis, in this case because of the very high value for the polarization resistance [15,16].

constant phase element (CPE) is substituted for the capacitive element to give a more accurate fit , as the obtain capacitive loop is depressed semicircle rather than regular one. The CPE is a special element whose impedance value is a function of the angular frequency (ω), and whose phase is independent of the frequency. Its admittance and impedance are, respectively, expressed as:

$$Y_{CPE} = Y_0(j\omega)^n \quad (1)$$

and

$$Z_{CPE}=(1/Y_0)[j\omega)_n]^{-1} \quad (2)$$

where Y_0 is the magnitude of the CPE, j is the imaginary number ($j^2 = -1$), a is the phase angle of the CPE and $n = \alpha/(\pi/2)$. The factor n is an adjustable parameter that usually lies between 0.5 and 1.0 . The CPE describes an ideal capacitor when n = 1. Values of a are usually related to the roughness of the electrode surface. The smaller value of α, the higher surface roughness. A good fit with this model was obtained with our experimental data. It is observed that the fitted data match the experimental, with an average error of about 1%.

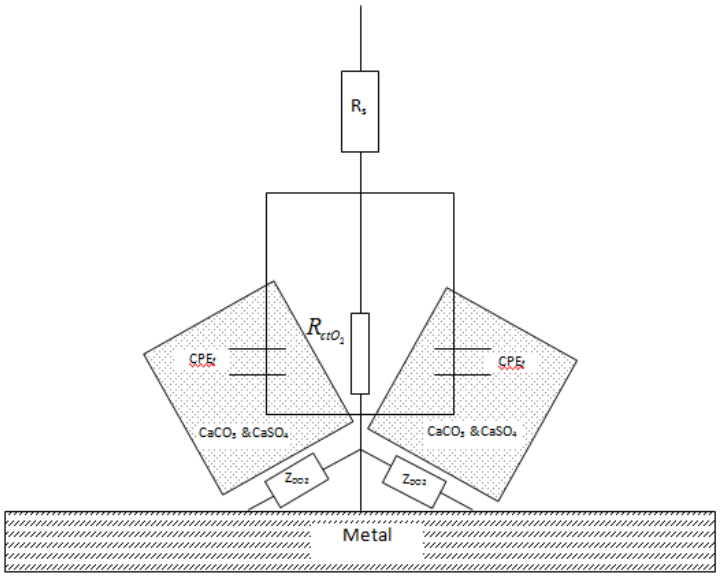

Figure 2. Equivalent circuit of the impedance diagrams in Fig. 1, in the presence of scales. R_s is the solution resistance, R_{ctO2} the charge transfer resistances of oxygen reduction , CPE_f is the constant phase element of scale film , Z_{DO2} is the diffusion impedance of oxygen.

The total capacitance loop in presence of scales is related to the polarization resistance of the scale film, the second time constant may attribute to the contribution of oxygen reduction occurs through the porous scale in cavities under the scale crystals by the charge transfer resistance R_{ctO_2} (Ωcm^2). The physical model can be illustrated by the equivalent circuit in Fig. 2 . The circuit was developed by Ben Amor [17] to explain the porous electrode model. Corrosion kinetic parameters derived from EIS measurements by fitting to suitable EC are given in Table 3. A higher polarization resistance in seawater and scale (R_{ct} = 33.72 Ωcm^2) compare to value of the sample in free seawater (R_{ct} = 25.06 Ωcm^2) typically corresponds to a lower corrosion rate. This also confirmed by decreasing in CPE value. This behavior associate with little increase in n value (~0.80), indicates that the CPE is little associate with the film capacitance processes.

The current vs potential curves for S41000 SS in seawater in absence and presence scales are shown in Fig. 3.

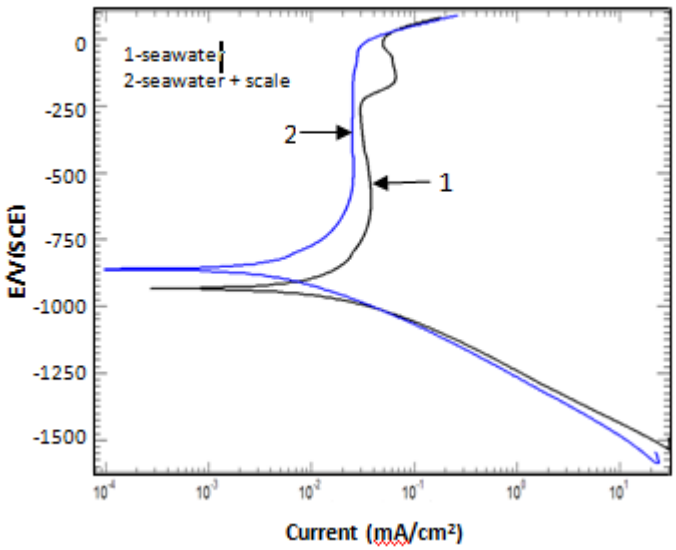

Figure 3. Potentiodynamic anodic and cathodic polarization curves S41000 SS in seawater without and with scale.

No change observed on the cathodic polarization curves in both cases. In the anodic part, Tafel region fallowed by a wide constant and low current plateau, which correspond to a passivation region, which mean that the S41000 SS spontaneously passivated in this condition. Two passive ranges was observed in anodic curves in case of seawater free of scale, the first wide passive region was started at -638 mV(SCE) which dissolved at -233 mV (SCE). The second narrow passive range was observed at -146 mV (SCE) and dissolved at -11 mV(SCE). This behavior may be due to formation of a passive film in the first region which may dissolved at high potential then another passive layer build up which dissolve as potential increase. In the case of scale presence, stable single wide passive region was observed.

Taking into account the following elementary reactions of corrosion process:

The reaction of S41000 SS dissolution (anodic process)

$$Fe \rightarrow Fe^{2+} + 2\bar{e} \quad (3)$$

Two cathodic process can suggested in this case [18]

- Reduction of the dissolved oxygen (I_{O_2}),

$$O_2 + 2e + 2H_2O \Leftrightarrow H_2O_2 + 2OH^- \quad (4)$$

$$H_2O_2 + 2e \Leftrightarrow 2OH^- \quad (5)$$

- Reduction of water (I_{H_2O}),

$$2H_2O + 2e \Leftrightarrow H_2 + 2OH^- \quad (6)$$

The total cathodic current (I_{total}),

$$I_{total} = I_{O_2} + I_{H_2O} \quad (7)$$

The rate of the corrosion process is determined by the corrosion current density (i_{corr}) obtained by extrapolating the anodic and cathodic Tafel lines to the corrosion potential E_{corr} of the working electrode and listed in Table 3 . The positive shift in E_{corr} and the lower I_{corr} suggested to produce stable non porous passivation scale on the S41000 SS surface.

Corrosion inhibition percentage efficiencies (IE.%) of the corrosion rate was calculated as follows:

$$IER_{ct}\% = \frac{(R_{ct})^{-1} - (R_{ct(inh.)})^{-1}}{(R_{ct})^{-1}} x100 \quad \textbf{(8)}$$

$$IEI_{corr.}\% = \frac{i_{corr.} - i_{corr.(inh.)}}{i_{corr.}} x100 \quad (9)$$

where R_{ct} , $i_{corr.}$ and $R_{ct(inh.)}$, $i_{corr.(inh.)}$ are the values of charge transfer resistance and corrosion current densities without and with scale, respectively

It is observed from data of Table 3 that (IE.%) calculated by impedance and polarization measurements are about $IE.R_{ct}\% = 25.68\%$ and $IE.I_{corr.}\% = 22.52\%$ respectively.

3.2 Effect of additives

Fig. 4,a represents a complex plane impedance plot recorded for S41000 SS with additives. It follows from Fig. 4,a depressed semicircle. This semicircle is attributed to the time constant of charge transfer and double layer capacitance and it follows by pseudo inductive loop.

The presence of yeast increase R_{ct} values about 1.82 time than in sea water, where Tyr increase the S41000 SS resistance about 1.5 time. The pseudo inductive loop observed at very low frequency of Nyquist spectra may due to the competitive between the localizes attack and hilling the weak points. The increase in the capacity (CPE) of the scale layer in presence of PAA and Try reflex the increase in the porosity of the scale film. The aggressive ions diffuse through this layer and reach the S41000 SS at S41000 SS / scale interface.

Bode plots, Fig.4,b, explains two times constant with phase angle Θ_{max} approach to 65º. This reflects the occurrence of two process, the first at which is corrosion process at high frequency, and

the second may the adsorption of scales. The data in presence of inhibitors fitted to the equivalent circuit in Fig.5. The protective action of the additive is clearly observed by R_{ct} and IE.R_{ct}% values in the Table 3, which give in the following order: Tyr < PAA< Yeast.

Polarization curves estimated in presence of additives are shown in Fig. 6. As can seen from this figure and corresponding data in Table 3 that $I_{corr.}$ values decreased and a clearly shift in E_{corr} towered anodic direction was observed. This behavior indicated enhancement of precipitation and adsorption process on the S41000 SS.

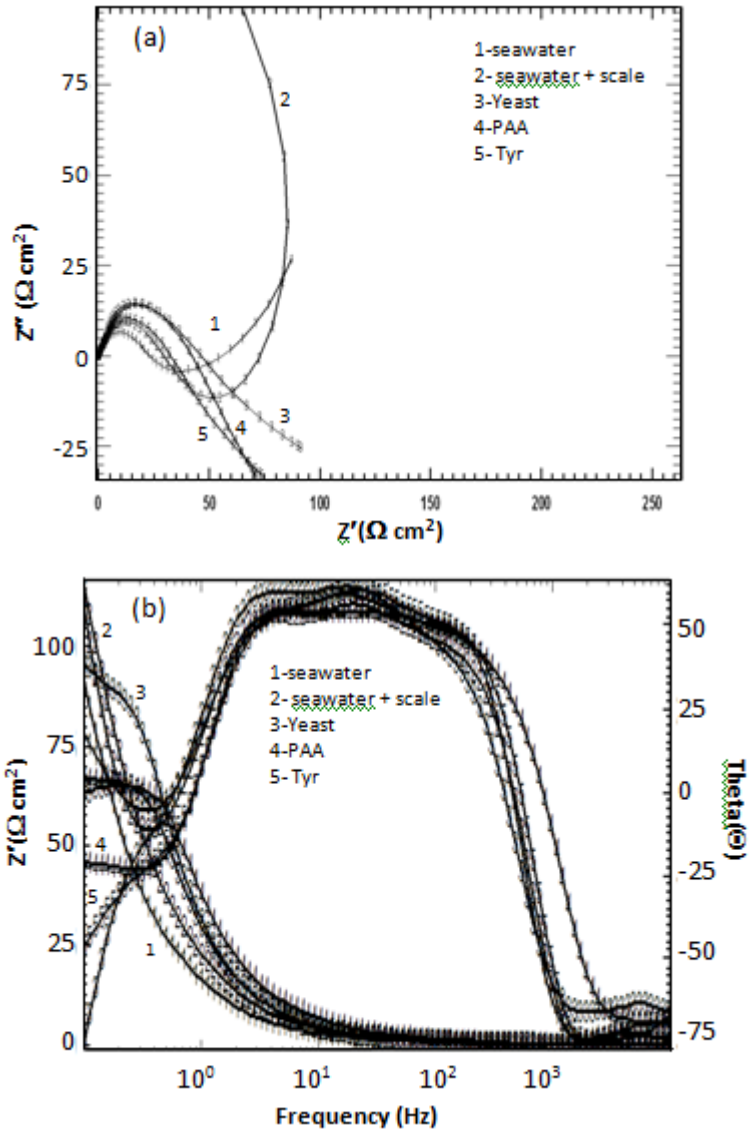

Figure 4. Impedance diagrams in Nyquist and bode plane plotted for S41000 S in seawater in presence of different additives.

The cathodic polarization curves are shifted towards increase in cathodic reaction in the presence of Tyr but it is still lower than in the additives free solution. In the anodic part, Tafel region fallowed by a wide constant and low current plateau, which correspond to a passivity region. This mean that the S41000 SS spontaneously passivated in the additives presence. It is clear

from Table 3 that the lower value of corrosion rate (I_{corr}) was observed in the presence of yeast (0.659 mA/cm2) which mean good agreement between impedance and polarization measurements.

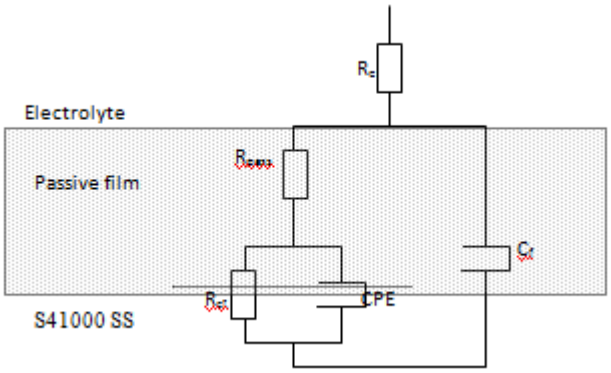

Figure 5. Electrical equivalent circuit for the interpretation of experimental impedance diagrams in presence the additives . R_{pass}: electrolytic resistance through the passive film; C_f : film capacity; R_{ct}: charge transfer resistance; CPE; double layer capacity.

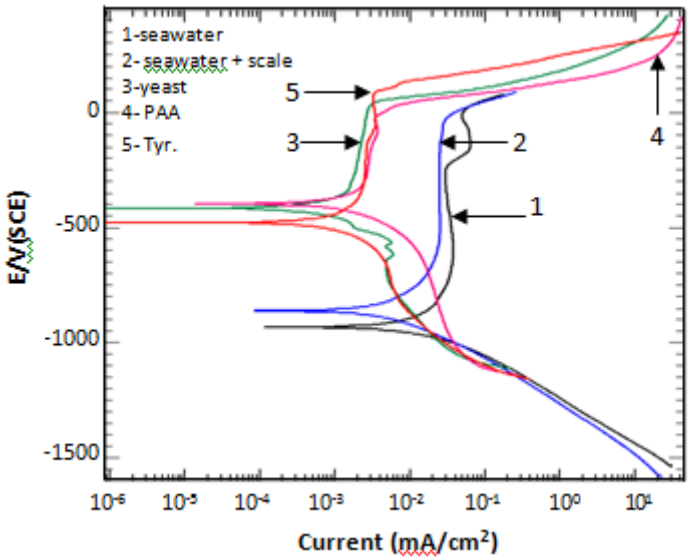

Figure 6. Potentiodynamic anodic and cathodic polarization curves S41000 SS in sea water in presence of different additives.

The scale inhibition capability of additives is related to chemical structure, molecular weight, active functional groups and solution pH – parameters that have been studied in depth by several investigators [19-21]. Inhibition phenomena do not entail chemical reactions and stem from complex physical processes, involving adsorption, nucleation and crystal growth processes. The fundamentals of inhibition mechanisms, particularly from their quantitative aspects, are poorly understood so that the effects on inhibition effectiveness are largely unpredictable. The same idea in the case of corrosion inhibition mechanism of metals which mainly depend on structure of the inhibitor and adsorption

ability of inhibitor molecule on the metal. According to this, the beneficial effect of yeast as anticorrosion compare with PAA and Tyr is due to its composition. A notable feature of yeast is the large proportion of nitrogenous substances which it contains. In general more than one-half of the dry yeast consists of proteins and other nitrogenous bodies (glycogen, gum, mucilage, fat, resinous matters, and cellulose) together with a good proportion of mineral ingredients [22]. These compounds have many functional groups, aromaticity, the possible steric effects, double bonds and lone pair electrons (such as the lone pairs electrons of nitrogen, sulfur, and oxygen atom) that facilitates the interaction between the these compounds and S41000 SS surface or scale nucleation .

3.3. Temperatures effect

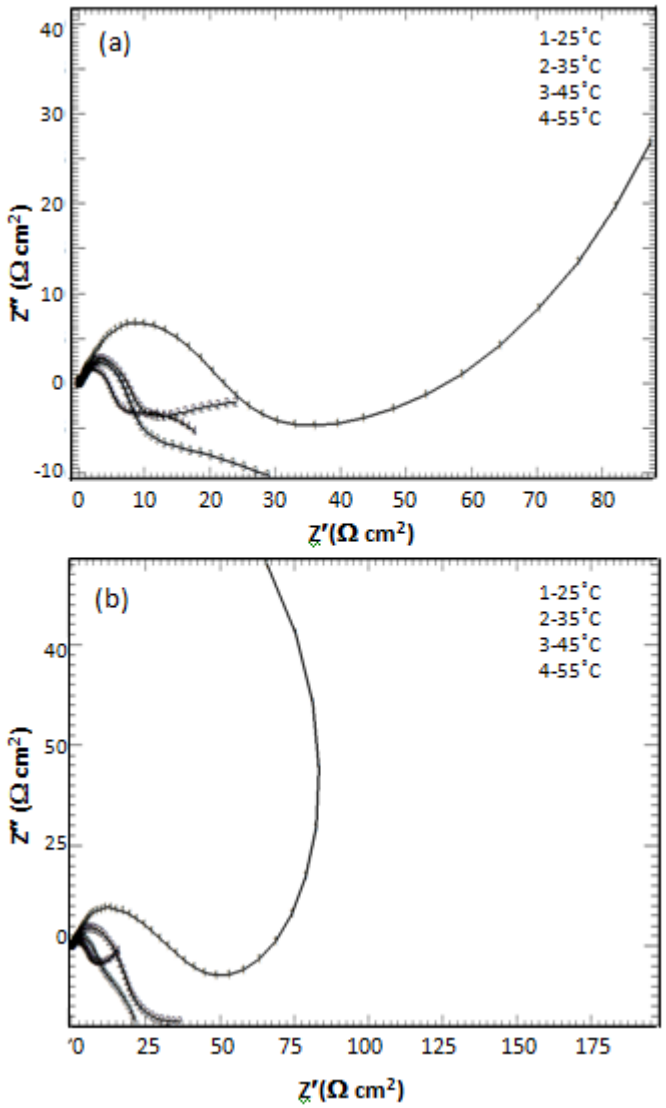

Figure 7. Impedance plots of S41000 SS at different temperatures in seawater. (a) without , (b) with scales.

Fig.7,a, shows the impedance spectra for the investigated S41000 SS in seawater at different temperatures. Capacitive arc `follows by diffusion tails was observed in all Nyquist

spectral in study temperatures range. It is clearly observed that as the temperatures increase from 25ºC to 55ºC the diameter of the capacitive loop is decreased (decrease in R_{ct} values and increase in CPE values). The diffusion tails at low frequencies concern the diffusion behavior in this range. The low value of Θ_{max} at high temperatures reflex the low ability of S41000 SS to produces protective layer on it. The values of n obtained in absence of scales indicated that the CPE is little associated with the film capacitance processes, certainly at high temperatures.

In presence of scale, impedance plots for S41000 SS at different temperatures the Nyquist diagrams (Fig.7,b) have the same features as in the absence of scale. S41000 resistance decreases as the temperatures increase at studied range associated to CPE increase.

Depressed capacitive loop with inductive tails was observed at 25 and 55 ºC, which indicate diffusion of iron ions throw porous scale layer takes place on S41000 alloy. Completive process between dissolution and scale precipitation process was observed at 35 and 45 ºC. Helalizadeha et al.[23] reveled that both $CaCO_3$ and $CaSO_4$ salts have inverse solubility behavior where the solubility decreases with increasing temperature and salts precipitate on heat exchange surfaces when the solution becomes supersaturated. Un complete coverage of S41000 SS surface by the precipitated scale may cause the low resistance of the alloy to aggressive solution. The R_{ct} value is about 7.8 time lower than it values at 25ºC. Also similar roughness degree (n values) was observed in absence and presence of scale specially at high temperature.

4. CONCLUSION

Tyrosine (Tyr), polyacrylic acid (PAA) and yeast were used in this study. They lead to modifications in the electrochemical behavior of S41000 SS in presence of artificial sea water and mixed salts - scales. Analyzing electrochemical data the following conclusions can be withdrawn:

1- S41000 SS does not suffer pitting corrosion in the artificial sea water .

2- Scale deposition on the metal moved the resistive / capacitive response toward resistance behavior with the oxygen reduction under scale layer.

3- In the experimental conditions presented above, it was shown that the stationary reduction current was the sum of two cathodic contributions, the limiting current of the oxygen reduction and the current of water reduction.

4- The difference in the inhibition actions for the corrosion of S41000 SS in presence scale formation of Tyr , PAA and yeast can be attributed to their composition.

5- Beneficial effect of yeast as anticorrosion as observed clearly from the electrochemical values compare with PAA and Tyr is due to its composition.

6- The passive region obtained in presence of additives are wider due to compact protective layer formed on the S41000 SS .

7- At temperature in the range of 35-55°C, diffusion behavior was observed on bare electrode and convert to completive process between dissolution of metal and scale precipitation process in presence of artificial sea water.

References

1. Wangnick, K., (1998), Worldwide desalting plants inventory report No. 15, USA, Wangnick Consultants.
2. S.K. Hamdona, R.B. Nessim, S.M. Hamza, *Desalination*, 94(1)(1993) 69.
3. D.J. Choi, S. J. You, J. G. Kim, *Mater. Sci. & Eng*. A, 335(1–2) (2002) 228.
4. S. K. Hamdona , O.A. Al Hadad, *Desalination*, 228 (2008) 277
5. M. Finsgara, S. Fassbenderb, S. Hirthc, I. Miloseva, *Mater. Chem. & Phy*., 116 (2009) 198–206
6. T.Y. Soror ,*The Open Corr. J*., 2(2009) 45.
7. S.Baraka-Lokmane, K.S. Sorbie, N. Poisson, ,P. Lecocq, In: Intenational Symposium of the Society of Core Analysts, 29 Oct - 02 Nov 2008, Abu Dhabi, United Arab Emirates.
8. B. Ghosh, S. S Kundu, B. Senthilmurugan , M. Haroun, *Int. J. Petrol. Sci. Tech*., 3(1) (2009)51.
9. J. A. Mikroyannidis, *Phosphorus Sulfur Relat. Elem*., 32(1987)113.
10. Q .Cheng , MG. Steinmetz , V. Jayaraman , *J. Am. Chem. Soc*., 124(26)(2002)7676.
11. S. Baraka-Lokmane, K.S. Sorbie, *Int. J. Petrol. Sci. Eng*., 70,(1–2)(2010)10.
12. M.A. Mahmoud , H.A. Nasr-El-Din, C.A. De Wolf, J.N. LePage, J.H. Bemelaar, *Soc. of Petrol. Eng*., 16(2011) 559.
13. K. H. Khoo, R. W. Ramette, C. H. Culberson, R. G. Bates, *Anal. Chem*., 49 (1977) 29.
14. I. Bentova, M. Bojinov, T. Tzvetkoff, *Electrochim. Acta*, 49 (2004) 2295
15. M.Slemnik, V. Dolecek, M. Gaberscek, *Acta Chim. Slov.*, 49 (2002) 613.
16. S .T. Arab, K. M. Emran, H. A .Al-Turaif *J. Saudi Chem. Soc.*, *In Press*(2011), Accepted Manuscript, Available online 12 June. http://www.sciencedirect.com/science/article/pii/S1319610311001190
17. Y. Ben Amor, L. Bousselmi, B. Tribollet, E. Triki, *Electroch. Acta*, 55 (2010) 4820.
18. O.Devos, C. Gabrielli, B.Tribollet, *Electrochim. Acta*, 51(2006) 1413.
19. Weijen and G.M. van Rosmalen, *Desalination*, 54 (1985) 239.
20. M.E. Tadros and I. Mayes, Linear growth rates of calcium sulfate dihydrate crystals in the presence of additives, *J. Colloid Interface Sci*., 72(2) (1979) 245.
21. A.E. Austin, J.F. Miller, D.A. Vaughan and J.F. Kircher, Chemical additives for calcium sulfate scale control, *Desalination*, 16 (1975) 345
22. http://chestofbooks.com/food/beverages/Alcohol-Properties/Composition-Of-Yeast.html.
23. A. Helalizadeha, H. Müller-Steinhagen, M. Jamialahmadi, *Chem. Eng. Sci*., 60(2005)5078.